



**Measurement of the $t\bar{t}$ Production cross section
at $\sqrt{s} = 1.96$ TeV in Dilepton Final States Using 1 fb^{-1}**

The DØ Collaboration
(Dated: March 13, 2007)

We present a measurement of the top quark pair ($t\bar{t}$) production cross section in $p\bar{p}$ collisions at $\sqrt{s} = 1.96$ TeV using events with ee , $e\mu$ or $\mu\mu$ final states. This analysis utilizes an integrated luminosity of approximately 1 fb^{-1} collected with the DØ detector at the Fermilab Tevatron collider. The cross sections measured separately in each of the three flavor channels as well as the combined cross section are:

$$\begin{aligned} ee &: \quad \sigma_{t\bar{t}} = 9.6_{-2.7}^{+3.2} \text{ (stat)} \quad {}_{-1.6}^{+1.9} \text{ (syst)} \pm 0.6 \text{ (lumi) pb;} \\ e\mu &: \quad \sigma_{t\bar{t}} = 6.1_{-1.2}^{+1.4} \text{ (stat)} \quad {}_{-0.7}^{+0.8} \text{ (syst)} \pm 0.4 \text{ (lumi) pb;} \\ \mu\mu &: \quad \sigma_{t\bar{t}} = 6.5_{-3.2}^{+4.0} \text{ (stat)} \quad {}_{-0.9}^{+1.1} \text{ (syst)} \pm 0.4 \text{ (lumi) pb;} \\ \text{dilepton} &: \quad \sigma_{t\bar{t}} = 6.8_{-1.1}^{+1.2} \text{ (stat)} \quad {}_{-0.8}^{+0.9} \text{ (syst)} \pm 0.4 \text{ (lumi) pb.} \end{aligned}$$

Preliminary Results for Winter 2007 Conferences

I. INTRODUCTION

The top quark is the heaviest fermion, and its mass could allow it to decay into exotic particles, e.g. a charged Higgs boson [1]. The inclusive top pair ($t\bar{t}$) production cross section ($\sigma_{t\bar{t}}$) can be computed from individual $t\bar{t}$ decay channels and their predicted standard model branching ratios. Exotic top decays would lead to different values of the inclusive top pair production cross section in the different channels. It is therefore important to precisely measure $\sigma_{t\bar{t}}$ in all channels and compare the results with the standard model predictions. Within the standard model each top quark of a $t\bar{t}$ pair is expected to decay approximately 99.8% of the time to a W boson and a b quark [2]. Dilepton final states arise when both W bosons decay leptonically and occur along with two energetic jets resulting from the hadronization of the b quarks. The detector signature includes missing transverse energy (\cancel{E}_T) from the high transverse momentum (p_T) of the W bosons' daughter neutrinos. The standard model $t\bar{t}$ branching fractions are 1.58%, 3.15%, and 1.57% [2] for the e^+e^- , $e^\pm\mu^\mp$ and $\mu^+\mu^-$ channels, respectively.

The $t\bar{t}$ production cross section in $p\bar{p}$ collisions has been measured in dilepton final states using the datasets provided by Run II of the Tevatron [3]. The updated $D\bar{O}$ measurements presented here are based on data taken in the period between April 2002 and February 2006 which corresponds, after data quality selection, to a measurement luminosity [4] of 1.04 fb^{-1} , 1.05 fb^{-1} and 1.05 fb^{-1} in the e^+e^- , $e^\pm\mu^\mp$ and $\mu^+\mu^-$ channels, respectively.

II. LEPTON AND JET IDENTIFICATION

The $D\bar{O}$ detector has a silicon microstrip tracker and a central fiber tracker located within a 2 Tesla(T) superconducting solenoidal magnet [5]. Surrounding the tracker is a liquid-argon/uranium sampling calorimeter consisting of a central cryostat covering pseudo-rapidities (η) up to ± 1.1 [6], and two end cryostats extending coverage to $|\eta| \approx 4$ [7]. A muon system [8] resides beyond the calorimeter, and consists of a layer of tracking chambers and scintillation trigger counters before 1.8 T toroidal magnets, followed by two more chamber layers. Luminosity is measured using plastic scintillator arrays located in front of the end cryostats.

Electrons are identified as clusters of energy in calorimeter cells in a cone of size $\Delta R \equiv \sqrt{\Delta\phi^2 + \Delta\eta^2} = 0.4$. Electron candidates are required to have a large fraction of their energy deposited in the electromagnetic layers of the calorimeter. The clusters are required to be isolated from hadronic energy deposition, to have a cluster-matched charged track in the central tracking system and to have a shower shape consistent with that of an electron. Before the shower shape requirement, electron candidates are referred to as “loose electrons”. We use both central ($|\eta| < 1.1$) and forward ($1.5 < |\eta| < 2.5$) electron candidates. In addition, we require the electrons to be selected by a likelihood discriminant that combines information both from the central tracking system and from the calorimeter in order to select prompt electrons. Electrons that meet all of these requirements are referred to as “tight electrons”.

Muons begin as a track segment in the inner muon layer which has been matched to segment formed from hits in the outer two muon layers. A track in the central tracking system must also match the muon identified in the muon system track, and the chi-squared of the overall track fit (χ^2) must be smaller than 4. To reject cosmic muons we apply cuts on the time of arrival of the muon track at the different layers of scintillators in the muon system. All muons must be found within $|\eta| < 2.0$. Muons supposedly originating from W (or Z) decay are identified using two isolation criteria: (i) the energy deposited in the calorimeter in a hollow cone around the muon track direction is smaller than 10% of the energy of the muon itself (this fraction is referred to as “calorimeter isolation”), and (ii) the scalar sum of the momenta of the charged tracks surrounding the muon track in the central tracking system is smaller than 10% of the muon track p_T (this fraction is referred to as “tracker isolation”). In the $e^\pm\mu^\mp$ channel both the calorimeter isolation and the tracker isolation criteria are relaxed to 15%. To select prompt muons we also require that the distance of closest approach of the muon track with respect to the primary vertex is smaller than 0.02 cm for a muon track with a hit in the silicon microstrip tracker and smaller than 0.2 cm for a muon track without a hit in the silicon microstrip tracker.

Jets are reconstructed with a fixed cone of radius, $\Delta R = 0.5$ [9] and must be recognized as such by the independent calorimeter trigger readout. Jet energy calibration is applied to the jets [10]. The \cancel{E}_T is equal in magnitude and opposite in direction to the vector sum of the transverse energies in all calorimeter cells for which the energy is significantly above the noise. The transverse momenta of electrons and isolated muons, as well as the jet energy calibration are taken into account in the calculation of \cancel{E}_T .

III. EVENT SELECTIONS

We select events requiring that they pass a dielectron trigger for the e^+e^- channel, an electron-plus-muon trigger for the $e^\pm\mu^\mp$ channel or a single muon trigger for the $\mu^+\mu^-$ channel. Offline, we select events with at least two jets

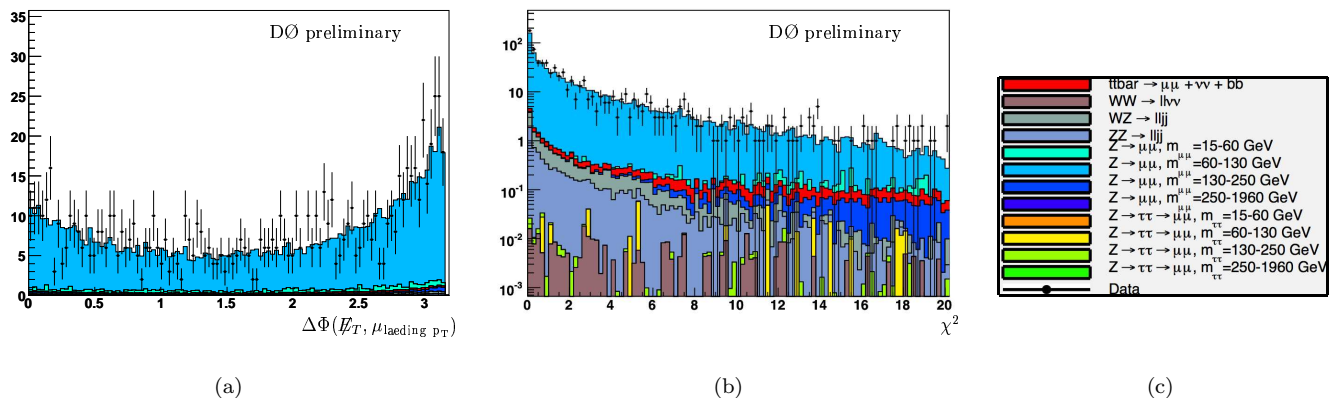


FIG. 1: (a) Distributions of $\Delta\phi$ between \cancel{E}_T and the leading muon μ_1 ; (b) the χ^2 computed from the fit of the di-muon mass to a Z -mass hypothesis for $\mu^+\mu^- + \geq 2$ jet events. The data (points) are compared to the MC expectation; (c) The color code of the different contributions for plots (a) and (b).

for the e^+e^- and $\mu^+\mu^-$ channels and at least one jet in the $e^\pm\mu^\mp$ channel. Each of the qualifying jets must have transverse momentum $p_T^j > 20$ GeV and $|\eta| < 2.5$ [6]. We also require two charged leptons ℓ with $p_T^\ell > 15$ GeV. Muons are accepted if in the region $|\eta| < 2.0$, while electrons must be within $|\eta| < 1.1$ or $1.5 < |\eta| < 2.5$. The two leptons are required to be of opposite charge in all three channels. The large missing transverse energy due to the neutrinos in the $t\bar{t}$ events is a powerful discriminant against background processes without high p_T neutrinos, such as $Z/\gamma^* \rightarrow \ell\ell$ where the ℓ is either an electron or a muon. In the e^+e^- channel, we veto events with a dielectron invariant mass $M_{ee} \leq 15$ GeV or $80 \leq M_{ee} \leq 100$ GeV and require $\cancel{E}_T > 35$ GeV ($\cancel{E}_T > 40$ GeV) for $M_{ee} > 100$ GeV ($15 < M_{ee} < 80$ GeV). In the $e^\pm\mu^\mp$ channel we do not apply any cut on the \cancel{E}_T , while in the $\mu^+\mu^-$ channel, we accept events with $\cancel{E}_T > 35$ GeV. The \cancel{E}_T cut is tightened when the azimuthal distance between the leading p_T muon (μ_1) direction and the direction of the \cancel{E}_T $\Delta\Phi(\cancel{E}_T, \mu_1)$ is large or small. Events with $\Delta\Phi(\cancel{E}_T, \mu_1) > 175^\circ$ are removed. Figure 1 (left) shows the predicted and observed $\Delta\Phi(\cancel{E}_T, \mu_1)$ distribution in $\mu^+\mu^- + \geq 2$ jet events.

The final selection in the $e^\pm\mu^\mp$ channel requires $H_T^i = p_T^{\ell_1} + \Sigma(p_T^j)$ to be greater than 115 GeV, where $p_T^{\ell_1}$ denotes the p_T of the leading lepton. This cut effectively rejects the largest backgrounds for this final state, which arise from $Z/\gamma^* \rightarrow \tau^+\tau^-$ and diboson production. The e^+e^- analysis uses a cut on sphericity $\mathcal{S} = 3(\epsilon_1 + \epsilon_2)/2$ to be greater than 0.15, where ϵ_1 and ϵ_2 are the two leading eigenvalues of the normalized momentum tensor [11]. This requirement rejects events in which jets are produced in a planar geometry through gluon radiation that is typical of background processes.

The final selection applied in the $\mu^+\mu^-$ channel further rejects the $Z/\gamma^* \rightarrow \mu^+\mu^-$ background. We compute for each $\mu^+\mu^-$ event the χ^2 of a fit to the $Z \rightarrow \mu^+\mu^-$ hypothesis given the measured muon momenta and known resolution. Figure 1 (middle) shows the predicted and observed χ^2 distribution in $\mu^+\mu^- + \geq 2$ jet events. Selecting events with $\chi^2 > 8$ is more effective than selecting on the dimuon invariant mass for this channel.

IV. SIGNAL EFFICIENCY

In order to compute the acceptances and efficiencies for the signal, we generate $t\bar{t}$ events at $\sqrt{s} = 1.96$ TeV using the ALPGEN [12] matrix element generator assuming a top mass m_{top} of 175 GeV. These events are processed through PYTHIA [13] to simulate fragmentation, hadronization and decays of short-lived particles. EVTGEN [14] is used to model the decays of b hadrons and TAUOLA [15] is used to model τ decays. The two W 's are made to decay to two lepton-neutrino pairs, including all τ final states. These events are processed through a full detector simulation using GEANT [16], which provides tracking hits, calorimeter cell energy and muon hit information. Extra $p\bar{p}$ interactions ‘noise’ (from data gathered with no trigger bias) is overlaid on all MC events, with the amount of activity determined by Poisson statistics given the instantaneous luminosities typically observed in the run. The same reconstruction process is then applied to both data and Monte Carlo (MC) events to determine various cut efficiencies.

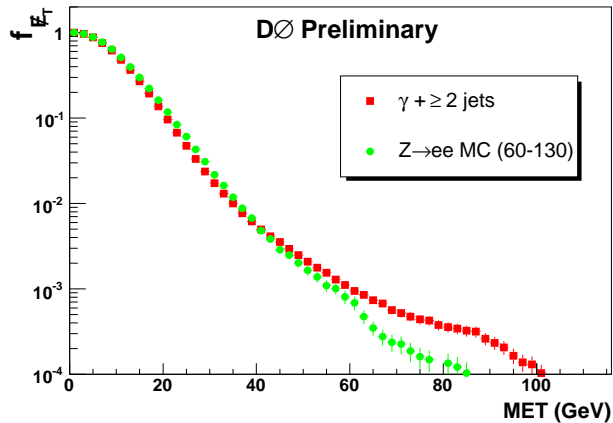


FIG. 2: Fake \cancel{E}_T rates observed in data ($\gamma + \geq 2$ jets) and MC ($Z \rightarrow ee$ in the mass range 60-130 GeV) samples.

V. BACKGROUND PROCESSES

Several background processes can fulfill the preselection criteria designed to select $t\bar{t}$. We distinguish two categories of backgrounds: “physics” and “instrumental”. Physics backgrounds are processes in which the charged leptons arise from electroweak boson decay and the \cancel{E}_T originates from high p_T neutrinos. This signature arises from $Z/\gamma^* \rightarrow \tau^+\tau^-$ where the τ leptons decay leptonically, and from WW/WZ (diboson) production. Instrumental backgrounds are defined as events in which (i) a jet or a lepton within a jet is misidentified as an isolated lepton (known as a ‘fake’ isolated lepton), or (ii) the \cancel{E}_T originates from misreconstructed jet or lepton energies or from noise in the calorimeter.

A. Physics backgrounds

The selection efficiencies for the physics backgrounds $Z/\gamma^* \rightarrow \tau^+\tau^- \rightarrow \ell\ell'$ with $\ell, \ell' = e$ or μ are estimated using Monte Carlo samples generated by ALPGEN and processed by PYTHIA while for WW/WZ they are estimated using PYTHIA. The $Z/\gamma^* \rightarrow \tau^+\tau^-$ and diboson + ≤ 2 jets processes are generated at leading order (LO) and are scaled by the factor of the next-to-next-to-leading order (NNLO) inclusive cross section divided by the LO inclusive cross sections [17, 18]. The correction leads to a cross section increase of 38% for the $Z/\gamma^* \rightarrow \tau^+\tau^-$ and of 40% for the diboson prediction. As the Z boson p_T is not properly described in the ALPGEN simulation, we reweighted the Z -boson p_T distribution for different jet multiplicity bins using $Z \rightarrow e^+e^-$ data events. We conservatively quote the ratio of the NNLO to LO diboson cross sections as the systematic uncertainty on the diboson background. The systematic uncertainty on the Z/γ^* contribution is estimated by varying the reweighting function within its uncertainties.

B. Fake missing E_T in $Z/\gamma^* \rightarrow ee, \mu\mu$

In the e^+e^- and $\mu^+\mu^-$ channels one primary background arises from fake \cancel{E}_T in $Z/\gamma^* \rightarrow ee, \mu\mu$ events. Detector resolutions can give rise to observed E_T imbalances in events which look like evidence of neutrinos. A contribution also arises from multijet production where both the ‘lepton’ and the ‘ \cancel{E}_T ’ are the result of mismeasurements rather than signatures from real leptons and neutrinos. Once the jet, electron, muon and scalar E_T resolutions of the Monte Carlo simulation have been adjusted to match the measured resolutions in data, we observe in both the e^+e^- and the $\mu^+\mu^-$ channels that the Monte Carlo \cancel{E}_T spectrum agrees well with that of the data when selecting a pure sample of $Z/\gamma^* \rightarrow ee, \mu\mu$ events in data.

In the e^+e^- channel, we determine the probability that processes without real high p_T neutrinos pass the \cancel{E}_T selection by measuring the ratio of the number of events above and below certain \cancel{E}_T threshold in $\gamma + 2$ jets candidate events. This sample is observed to have the same \cancel{E}_T distribution as $Z/\gamma^* \rightarrow ee$ Monte Carlo. The fake \cancel{E}_T rates observed in $\gamma + 2$ jets data and in MC are shown in Fig. 2. This probability is multiplied by the number of data events that fail the \cancel{E}_T selections but pass all other selections to get the number of fake missing E_T background events in the final selected sample.

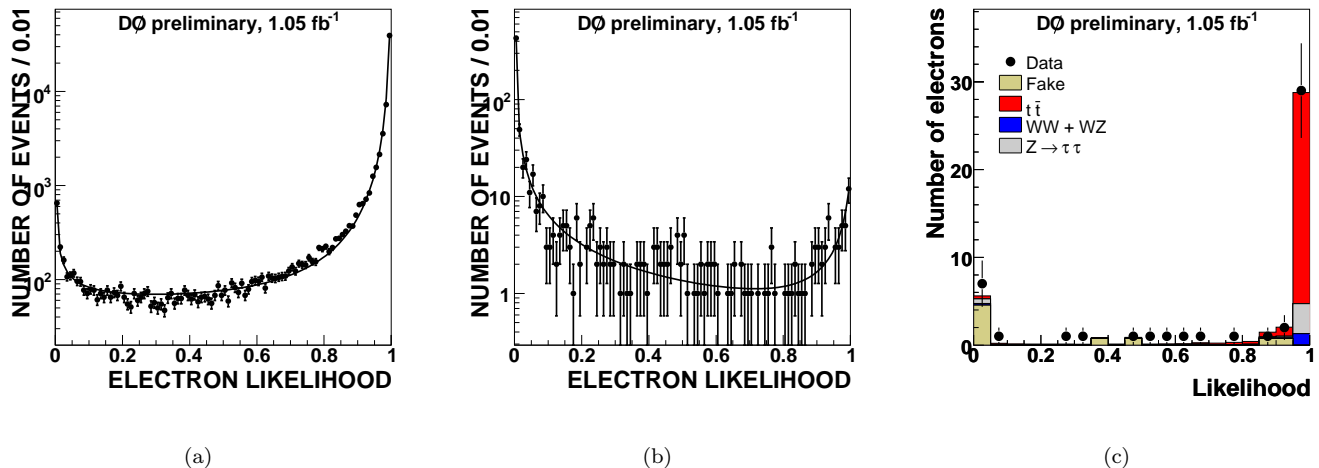


FIG. 3: (a) Electron likelihood distribution for electrons in $Z \rightarrow ee$ data events; (b) Misidentified electron likelihood distribution from the background data; (c) After the final selection cuts.

C. Misidentified electron background

Misidentified electrons can arise from instrumental effects. Jets comprised essentially of a leading π^0/η and an overlapping or conversion-produced track, for example, can mimic an isolated high- p_T electron. In the e^+e^- and $e^\pm\mu^\mp$ analyses the amount of misidentified electron background is fitted to the observed distribution of electron likelihood in the data. To this end we first determine the shape of the electron likelihood for real electrons in a pure $Z/\gamma^* \rightarrow e^+e^-$ sample. The shape of the electron likelihood for the misidentified electron background is determined using a sample dominated by misidentified electrons and selected in the following way:

- for the e^+e^- analysis, the event should contain a non-isolated EM cluster with bad track matching and poor shower shape, and a loose electron. The loose electron was used to study the electron likelihood shape;
- for the $e^\pm\mu^\mp$ analysis, the muon is required to be anti-isolated (both calorimeter and tracker isolation greater than 20%) and the event must have $\cancel{E}_T < 15$ GeV. The number of misidentified electrons in the selected $e^\pm\mu^\mp$ sample is obtained by performing an extended unbinned likelihood fit to the observed distribution of electron likelihood in data. The likelihood is given by:

$$\mathcal{L} = \prod_{i=1}^N (n_e S(x_i) + n_{misid} B(x_i)) \frac{e^{-(n_e + n_{misid})}}{N!},$$

where i is an index that runs over all selected events, x_i is the corresponding observed value of the electron likelihood, N is the total number of selected events, n_e is the number of events with an isolated electron, n_{misid} is the number of events with a misidentified electron, S is the signal probability distribution function determined using real electrons, and B is the background probability distribution function derived from the sample dominated by misidentified electrons. Figure 3 shows the shapes of the electron likelihood discriminant distributions in the real electron and misidentified electron samples, and in the analysis data.

D. Fake isolated muon background

An isolated muon can be impersonated by a muon in a jet when the jet is not reconstructed. We measure the fraction of muons (f_μ) that appear as isolated in a di-muon control sample dominated by fake isolated muons. To suppress physics processes with real isolated muons the leading p_T muon is required to fail the muon criteria. This efficiently cuts $Z/\gamma^* \rightarrow \mu^+\mu^-$ events but also cuts $W \rightarrow \mu\nu$ events where a second high p_T muon might arise from a muon in a jet. In the $\mu^+\mu^-$ channel, the number of events with a fake isolated muon contributing to the final

sample sample is estimated using the ‘matrix method’ [19] using two samples: the ‘tight’ sample requires two isolated muons; the “loose” sample requires only one isolated muon. In the $e^\pm\mu^\mp$ channel the contribution from events where both leptons are fake leptons is already accounted for when computing the misidentified electron background. The remaining contribution (from events with a real electron and a fake isolated muon) is computed from the number of events in a sample where the electron and the muon have the same sign and where there is no muon isolation requirement, times the previously measured fraction f_μ .

VI. PREDICTION AND OBSERVATION

In Table 1 we summarize the predicted and observed number of events. The prediction for Z/γ^* background, misidentified leptons, and diboson backgrounds are also provided. We observe a total of 73 events after the final selections with an expected background of 23.5 events. Predicted and observed distributions for various event variables are shown in Fig 4.

Category	ee	$\mu\mu$	$e\mu$ (≥ 2 jets)	$e\mu$ (1 jet)
integrated luminosity (pb^{-1})	1036	1046	1046	1046
Z/γ^*	$2.4^{+0.4}_{-0.4}$	$2.7^{+0.4}_{-0.4}$	$3.6^{+0.7}_{-0.8}$	$5.5^{+0.8}_{-0.8}$
WW/WZ and other MC	$0.4^{+0.2}_{-0.2}$	$0.5^{+0.1}_{-0.1}$	$1.4^{+0.6}_{-0.6}$	$3.4^{+1.4}_{-1.4}$
Instrumental background	$0.2^{+0.2}_{-0.1}$	$0.4^{+0.2}_{-0.2}$	$1.8^{+0.6}_{-0.6}$	$1.2^{+0.4}_{-0.4}$
Total background	$3.0^{+0.5}_{-0.5}$	$3.6^{+0.5}_{-0.5}$	$6.7^{+1.2}_{-1.2}$	$10.2^{+1.8}_{-1.7}$
Signal efficiency (%)	$8.3^{+1.2}_{-1.2}$	$5.1^{+0.4}_{-0.4}$	$12.4^{+0.9}_{-1.0}$	$3.1^{+0.3}_{-0.3}$
Expected signal	$9.5^{+1.4}_{-1.4}$	$5.8^{+0.5}_{-0.5}$	$28.6^{+2.1}_{-2.4}$	$7.1^{+0.6}_{-0.7}$
Total Sig. + Bkg.	$12.5^{+1.5}_{-1.5}$	$9.4^{+0.7}_{-0.7}$	$35.3^{+2.8}_{-3.2}$	$17.2^{+2.0}_{-2.1}$
Selected events	16	9	32	16

TABLE 1: Expected background and observed and expected signal event yields. The expected signal yield is derived assuming $\sigma_{t\bar{t}} = 7$ pb. The error on the each yield is the quadratic sum of the statistical and systematic uncertainties. For the e^+e^- ($\mu^+\mu^-$) channel, the $Z/\gamma^* \rightarrow ee$ ($Z/\gamma^* \rightarrow \mu\mu$) background, respectively, enters into the Z/γ^* contribution.

VII. RESULTS

The $t\bar{t}$ cross section in the individual dilepton channels is extracted by minimizing a negative log-likelihood function based on the Poisson probability of observing a number of events (N_j^{obs}) given the luminosity (\mathcal{L}_j), branching fraction (BR_j), efficiency (ϵ_j) and a number of background events (N_j^{bkg}): $-\log L(\sigma_j, \{N_j^{obs}, N_j^{bkg}, BR_j, \mathcal{L}_j, \epsilon_j\})$, while the combined cross section is measured by minimizing the sum of the negative log-likelihood functions for each individual channel (see [20] for more details on the method).

The preliminary $t\bar{t}$ production cross sections at $\sqrt{s} = 1.96$ TeV in dilepton channels for the top quark mass of 175 GeV are measured to be:

$$\begin{aligned}
ee : \quad \sigma_{t\bar{t}} &= 9.6^{+3.2}_{-2.7} \text{ (stat)} \quad {}^{+1.9}_{-1.6} \text{ (syst)} \pm 0.6 \text{ (lumi) pb;} \\
e\mu : \quad \sigma_{t\bar{t}} &= 6.1^{+1.4}_{-1.2} \text{ (stat)} \quad {}^{+0.8}_{-0.7} \text{ (syst)} \pm 0.4 \text{ (lumi) pb;} \\
\mu\mu : \quad \sigma_{t\bar{t}} &= 6.5^{+4.0}_{-3.2} \text{ (stat)} \quad {}^{+1.1}_{-0.9} \text{ (syst)} \pm 0.4 \text{ (lumi) pb;} \\
\text{dilepton} : \quad \sigma_{t\bar{t}} &= 6.8^{+1.2}_{-1.1} \text{ (stat)} \quad {}^{+0.9}_{-0.8} \text{ (syst)} \pm 0.4 \text{ (lumi) pb.}
\end{aligned}$$

The measured cross sections are in good agreement with the standard model prediction of 6.77 ± 0.42 pb [21]. Fig.5 shows the variation of the measured combined cross section as a function of top quark mass.

The systematic uncertainty on the dilepton cross section measurement is obtained by varying the efficiencies and background contributions within their errors, taking all the correlations between the channels and between the different classes of background into account. The dominant systematic uncertainties are summarized in Table 2. The following main systematics have been studied:

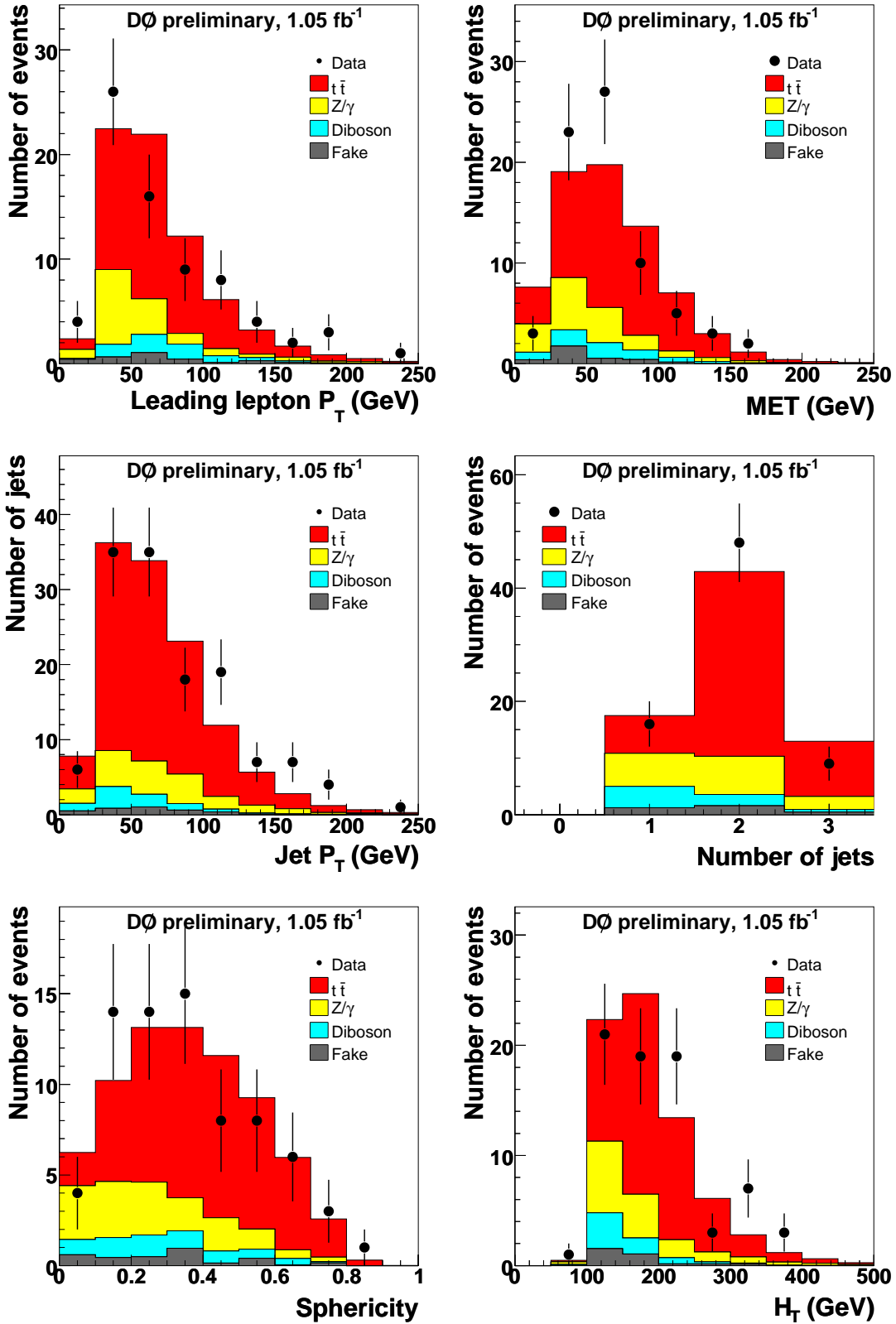


FIG. 4: Observed and predicted distributions for various backgrounds and the signal after the final selection cuts for the three dilepton channels. From top to bottom and left to right: leading lepton p_T ; missing transverse energy (MET or \cancel{E}_T); jet p_T ; number of jets (the last bin is inclusive); sphericity; H_T (scalar sum of leading lepton and two jet p_T).

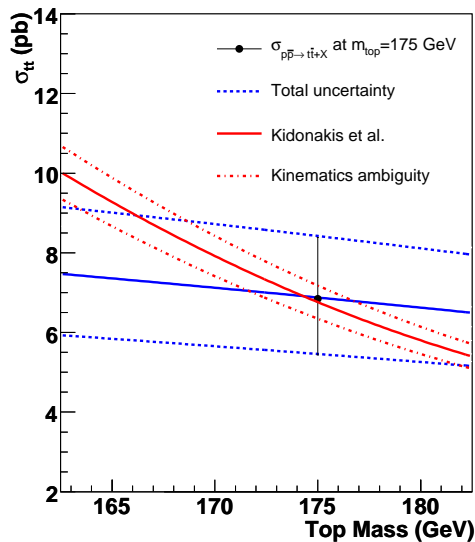


FIG. 5: Variation of the combined $t\bar{t}$ production cross section as measured in the dilepton channels (point) as a function of top quark mass (blue line). Red line shows the theoretical prediction from [21].

- **Jet energy calibration:** The measured jet energies in the calorimeter are corrected for the response of the calorimeter, for jet showering outside the jet reconstruction cone and for energy from underlying activity in the event [10]. The uncertainty on the jet energy calibration is propagated to the predicted background yields and to the efficiency for the $t\bar{t}$ signal.
- **Jet identification and resolution:** Jet reconstruction efficiency and jet resolution are determined in data and applied to Monte Carlo. Uncertainties related to the methods are propagated to signal and background predictions.
- **Primary vertex identification:** This uncertainty takes into account the difference observed in vertex distributions between data and Monte Carlo.
- **Lepton identification:** The lepton identification efficiencies are measured in the data using well understood processes. They are studied in various detector regions and various jet environments. Residual deviations from unity of the ratio of data to Monte Carlo efficiencies are used as systematic uncertainties. The electron identification systematic uncertainty is mainly due to the dependency on the number of jets and is conservatively estimated to be around 5.5%.
- **Trigger efficiency:** Trigger efficiencies are derived from the data. They have uncertainties due to limited sample statistics. Various sources of bias are investigated, and the resulting variations in trigger efficiencies are included as systematic errors.
- **Fake electron background in the $e\mu$ channel:** In the electron channel the shape of the electron likelihood discriminant is used to fit the number of fake electrons in the final selected sample. The shape itself is found to be dependent on the electron p_T and the detector occupancy (number of jets). The number of fake electron is fitted with the various shapes to extract this systematic uncertainty on the background.
- **MC background normalization:** The ratio of the NNLO cross section divided by the LO cross section which was used to scale the PYTHIA $WW/WZ/ZZ$ Monte Carlo cross sections is taken as the systematic uncertainty for the diboson background. The systematic uncertainty on the Z/γ^* background normalization is estimated varying the Z -boson p_T reweighting function.

Table 2 summarizes the systematic uncertainties in the cross section measurements. The Monte Carlo and fake backgrounds statistical uncertainties are treated as uncorrelated between channels. All other sources of systematic uncertainties are treated as correlated between channels. The jet energy scale uncertainty dominates the total systematic error.

Systematic Uncertainty Source (pb)	ee	$e\mu$ (≥ 1 jet)	$\mu\mu$	$\ell\ell$
Jet energy calibration	+0.4–0.4	+0.3–0.3	+0.7–0.2	+0.3–0.3
Jet identification	+0.1–0.0	+0.1–0.1	+0.1–0.3	+0.1–0.1
Primary vertex identification	+0.3–0.3	+0.3–0.2	+0.2–0.2	+0.3–0.2
Muon identification		+0.2–0.2	+0.5–0.4	+0.2–0.2
Electron identification	+1.4–1.2	+0.5–0.4		+0.6–0.5
Trigger	+1.0–0.8	+0.2–0.2	+0.3–0.3	+0.2–0.2
Fake background	+0.1–0.1	+0.3–0.3	+0.3–0.3	+0.2–0.2
MC normalization	+0.3–0.3	+0.3–0.3	+0.4–0.4	+0.3–0.3
Other	+0.5–0.4	+0.2–0.1	+0.4–0.4	+0.2–0.2
Total	+1.9–1.6	+0.8–0.7	+1.1–0.9	+0.9–0.8

TABLE 2: Summary of the systematic uncertainties on the $t\bar{t} \rightarrow \ell\bar{\ell}$ cross section measurements in pb.

VIII. ACKNOWLEDGEMENTS

We thank the staffs at Fermilab and collaborating institutions, and acknowledge support from the DOE and NSF (USA); CEA and CNRS/IN2P3 (France); FASI, Rosatom and RFBR (Russia); CAPES, CNPq, FAPERJ, FAPESP and FUNDUNESP (Brazil); DAE and DST (India); Colciencias (Colombia); CONACyT (Mexico); KRF and KOSEF (Korea); CONICET and UBACyT (Argentina); FOM (The Netherlands); PPARC (United Kingdom); MSMT (Czech Republic); CRC Program, CFI, NSERC and WestGrid Project (Canada); BMBF and DFG (Germany); SFI (Ireland); The Swedish Research Council (Sweden); Research Corporation; Alexander von Humboldt Foundation; and the Marie Curie Program.

-
- [1] J.F. Gunion *et al.*, *The Higgs Hunters Guide* (Addison-Wesley, Redwood City, California, 1990), p. 200.
- [2] S. Eidelman *et al.*, Phys. Lett. **592**, 1 (2004).
- [3] CDF Collaboration, D. Acosta *et al.*, Phys. Rev. Lett. **93**, 142001 (2004); DØ Collaboration, V. Abazov *et al.*, Phys. Lett. B **626**, 55 (2005).
- [4] T. Andeen *et al.*, FERMILAB-TM-2365-E (2006), in preparation.
- [5] DØ Collaboration, V. Abazov *et al.*, *The Upgraded DØ Detector*, Nucl. Instrum. and Methods Phys. Res. A, **565**, 463 (2006).
- [6] Rapidity y and pseudo-rapidity η are defined as functions of the polar angle θ and parameter β . Specifically, $y(\theta, \beta) \equiv \frac{1}{2} \ln[(1 + \beta \cos\theta)/(1 - \beta \cos\theta)]$, and $\eta(\theta) \equiv y(\theta, 1)$, where β is the ratio of a particle's momentum to its energy.
- [7] DØ Collaboration, S. Abachi *et al.*, Nucl. Instrum. and Methods Phys. Res. A, **338** 185 (1994).
- [8] V. Abazov *et al.*, *The muon system of the Run II D0 detector*, Nucl. Instrum. and Methods A **552**, 372 (2005).
- [9] Jets are defined using an iterative seed-based cone algorithm with $\Delta\mathcal{R} = \sqrt{(\Delta\phi)^2 + (\Delta\eta)^2} = 0.5$ (where ϕ is the azimuthal angle), including mid-points as described in Sec. 3.5 (p.47) of G. C. Blazey *et al.*, in *Proceedings of the Workshop: "QCD and Weak Boson Physics in Run II"*, edited by U. Baur, R. K. Ellis, and D. Zeppenfeld, FERMILAB-PUB-00-297 (2000).
- [10] DØ Collaboration, B. Abbott *et al.*, Nucl. Instrum. and Methods A **424**, 352 (1999).
- [11] V. Barger, J. Ohnemus, and R. J. N. Phillips, Phys. Rev. D **48**, 3953 (1993).
- [12] M.L. Mangano *et al.*, *ALPGEN, a generator for hard multiparton processes in hadronic collisions*, JHEP **307**, 001 (2003), hep-ph/0206293.
- [13] <http://www.thep.lu.se/torbjorn/Pythia.html>
T. Sjöstrand, T. Lönnblad, G. Miu, S. Mrenna and E. Norrbin, Comp. Phys. Commun. **135**, 238 (2001), hep-ph/0010017; see also T. Sjöstrand, T. Lönnblad, S. Mrenna and P. Skands, hep-ph/0308153.
- [14] D. J. Lange, Nucl. Instrum. and Methods Phys. Res. A **462**, 152 (2001).
- [15] S. Jadach *et al.*, Comp. Phys. Commun. **76**, 361 (1993).
- [16] R. Brun and F. Carminati, CERN Program Library Long Writeup W5013, 1993 (unpublished).
- [17] J.M. Campbell and R.K. Ellis, Phys.Rev.D **60**, 113006 (1999).
- [18] J.M. Campbell and R.K. Ellis, *MCFM - Monte Carlo for FeMtobarn processes*, <http://mcfm.fnal.gov>
- [19] DØ Collaboration, *Measurement of the $t\bar{t}$ Production Cross Section in $p\bar{p}$ Collisions Using Dilepton Events*, Phys. Rev. D, in preparation.
- [20] DØ Collaboration, *Combined $t\bar{t}$ Production Cross Section at $\sqrt{s} = 1.96$ TeV in the Lepton+Jets and Dilepton Final States using Event Topology*, DØ Note 4906, August 2005.
- [21] R. Bonciani *et al.*, Nucl. Phys. **B529**, 424 (1998); N. Kidonakis and R. Vogt, Phys. Rev. D **68**, 114014 (2003); M. Cacciari *et al.*, JHEP **404**, 68 (2004).